Supplementary information for

Spatial transcriptomic analysis drives PET imaging of tight junction protein expression in pancreatic cancer theranostics

James Wang*[1], Jai Woong Seo*[1], Aris J. Kare*[1,2], Martin Schneider[1], Mallesh Pandrala[1], Spencer K. Tumbale[1], Marina N. Raie[1], Gokce Engudar[1], Nisi Zhang[1], Yutong Guo[1], Xiaoxu Zhong[3], Sofia Ferreira[3], Bo Wu[1], Laura D. Attardi[3], Guillem Pratx[3], Andrei Iagaru[4], Ryan L. Brunsing[5], Gregory W. Charville[6], Walter G. Park[7], Katherine W. Ferrara[1,+]

Supplementary Methods

Supplementary Figures

Supplementary Tables

Supplementary Videos

Supplementary Methods

Synthesis of DOTA-PEG_2-C4BP: DOTA-PEG_2-NSSYSGNYYSIL-NH_2 was synthesized using standard Fmoc solid-phase peptide synthesis on Rink amide ChemMatrix resin (Biotage, 0.1 mmol scale). The coupling reaction utilized a programed sequential addition of amino acids (3 equivalents), a PEG spacer (3 equivalents), and a DOTA chelator (2 equivalents) in a microwave-assisted automated peptide synthesizer (Initiator+Alstra, Biotage). HBTU (2.8 equivalents) and DIPEA (6 equivalents) are used in each coupling step. After completion of the peptide synthesis cycle, the resin was washed with methanol and dried under vacuum. The resin was suspended in a mixture of TFA-H_2O-TIPS (95:2.5:2.5, v/v/v, total volume 5-6 mL) for 2.5 h. The peptide was purified on high performance liquid chromatography (HPLC) using 5−90% acetonitrile gradient with 0.1% TFA water. The purified product was confirmed by matrix-assisted laser desorption ionization (MALDI) mass spectrometry (AB Sciex 5800 MALDI TOF/TOF) under positive and reflective mode with sinapic acid matrix. [$M+H^+$, C83H125N20O31] calculated monoisotopic mass 1897.9, measured mass 1898.0. Abbreviation: HBTU (*N,N,N′,N′*-tetramethyl-*O*-(1*H*-benzotriazol-1-yl)uronium hexafluorophosphate), DIPEA (diisopropyethylamine), TFA (trifluoroacetic acid), TIPS (triisopropylsilane).

Xenograft mouse model: Xenograft tumors were established in both shoulders of NOD/SCID mice (Jackson Laboratory) by subcutaneous injection of Capan-1 cells (1×10^6) suspended in 1:1 Matrigel:DMEM medium (100 µL).

PET/CT imaging, ROI analysis, biodistribution of xenograft mice: The PET/CT imaging of xenograft NOD/SCID (Jackson Laboratory) mice (n=10) bearing Capan-1 tumors followed the scanning protocol in the Methods Section once tumor size reached ~5 mm diameter. PET/CT (Inveon, Siemens) scanning of mice started on the PET scanner bed with a simultaneous tail-vein injection of ^{64}Cu-C4BP in 10 seconds and following 1 hour, photon acquisition to obtain dynamic temporal images, then subsequently, CT imaging was acquired for 10 minutes for anatomical reference. Mice (n=4) received a tail vein injection of ^{64}Cu-C4BP (71±4.9µCi or 2.6±0.2 MBq/mouse). For blocking (n=6), injection of ^{64}Cu-C4BP (81±5.9µCi or 3.0±0.2 MBq/mouse) was proceeded with 500-fold excess cold compound (~0.12 mg/mouse). Accumulation of radioactivity (tumor, kidneys, and blood) was quantified by manually drawing regions of interest (ROI) after co-registration of PET/CT images on Inveon Research Workplace (IRW) software. Organ radioactivity was normalized to the percent injected activity per cubic centimeter (%IA/cc) volume. After PET/CT scanning, mice were awake for one hour and then euthanized; blood was perfused. Organs of interest were collected, and the radioactivity in each organ was measured using a gamma counter and calculated as percent injected activity per gram (%IA/g) in organs.

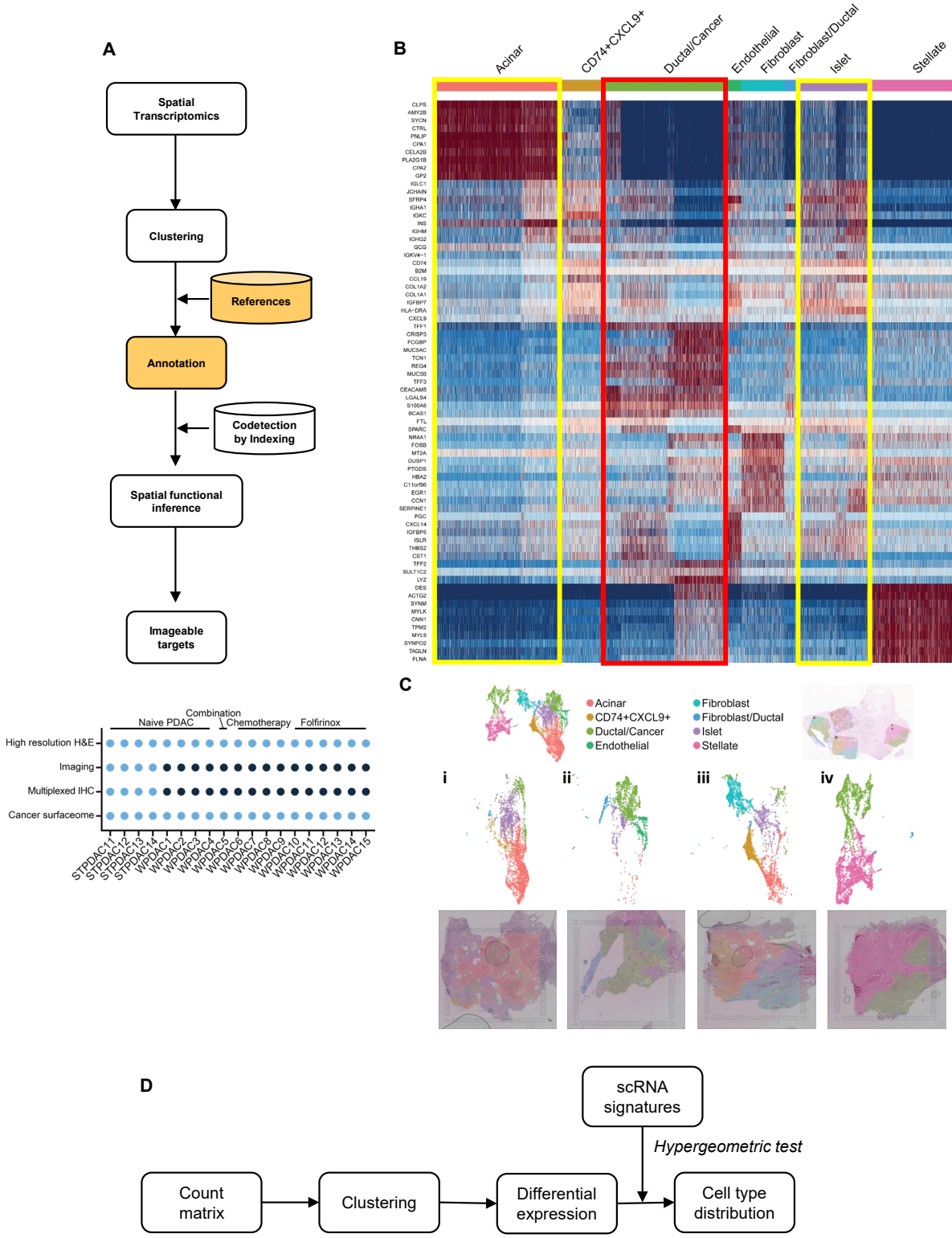
Western blot of CLDN4: The tumor cell lines Capan-1, PANC-1, mT4, and NDL were lysed in RIPA lysis buffer (ThermoFisher Scientific) for 10 minutes at 4 °C. After protein quantification via the bicinchoninic acid (BCA) assay, protein concentrations were standardized to 0.4 mg/mL. The homogenized protein samples were then combined with the loading buffers (ThermoFisher Scientific) per the manufacturer's guidelines, and 2 µg of each sample was loaded per well on an SDS-PAGE gel. Following SDS-PAGE separation, proteins were transferred to a PVDF membrane (ThermoFisher Scientific). For protein detection, the membrane was stained with primary antibodies: a rabbit polyclonal antibody against CLDN4 (1:200 dilution, ThermoFisher Scientific, Catalog #36-4800) and a rabbit antibody against β-actin (1:2000 dilution, Sigma Aldrich). Primary antibody bound to each protein was stained by incubation with a secondary goat anti-rabbit IgG (H+L) antibody conjugated with horseradish peroxidase (HRP) (1:2000 dilution, Thermo Fisher Scientific). Visualization of protein bands was done using a chemiluminescence substrate (BioRad) and imaging system (BioRad, ChemiDoc XRS+ CCD) for subsequent analyses.

Immunohistochemistry of CLDN4*:* Harvested tissues were fixed with 10% formalin solution for more than 24 hours and then processed using the standard paraffin embedded tissue sectioning procedure by the UC Davis Center for Genomic Pathology Lab. Briefly, antigen retrieval was performed for 45 min with a citrate buffer at pH 6.0 in a Decloaking Chamber (Biocare Medical, Concord, CA) at 125°C and 15 psi. Slides were blocked with normal goat serum then incubated with a hCLDN4 polyclonal rabbit antibody (1:200, ThermoFisher Scientific, Catalog #36-4800) overnight at room temperature in a humidified chamber, followed by a biotinylated goat anti-rabbit secondary antibody (1:1000, Vector Labs, BA-1000-1.5). The Vectastain ABC Elite Kit and a diaminobenzidine Peroxidase Substrate Kit (Vector Labs, Burlingame, CA) were used for amplification and visualization of signal, respectively.

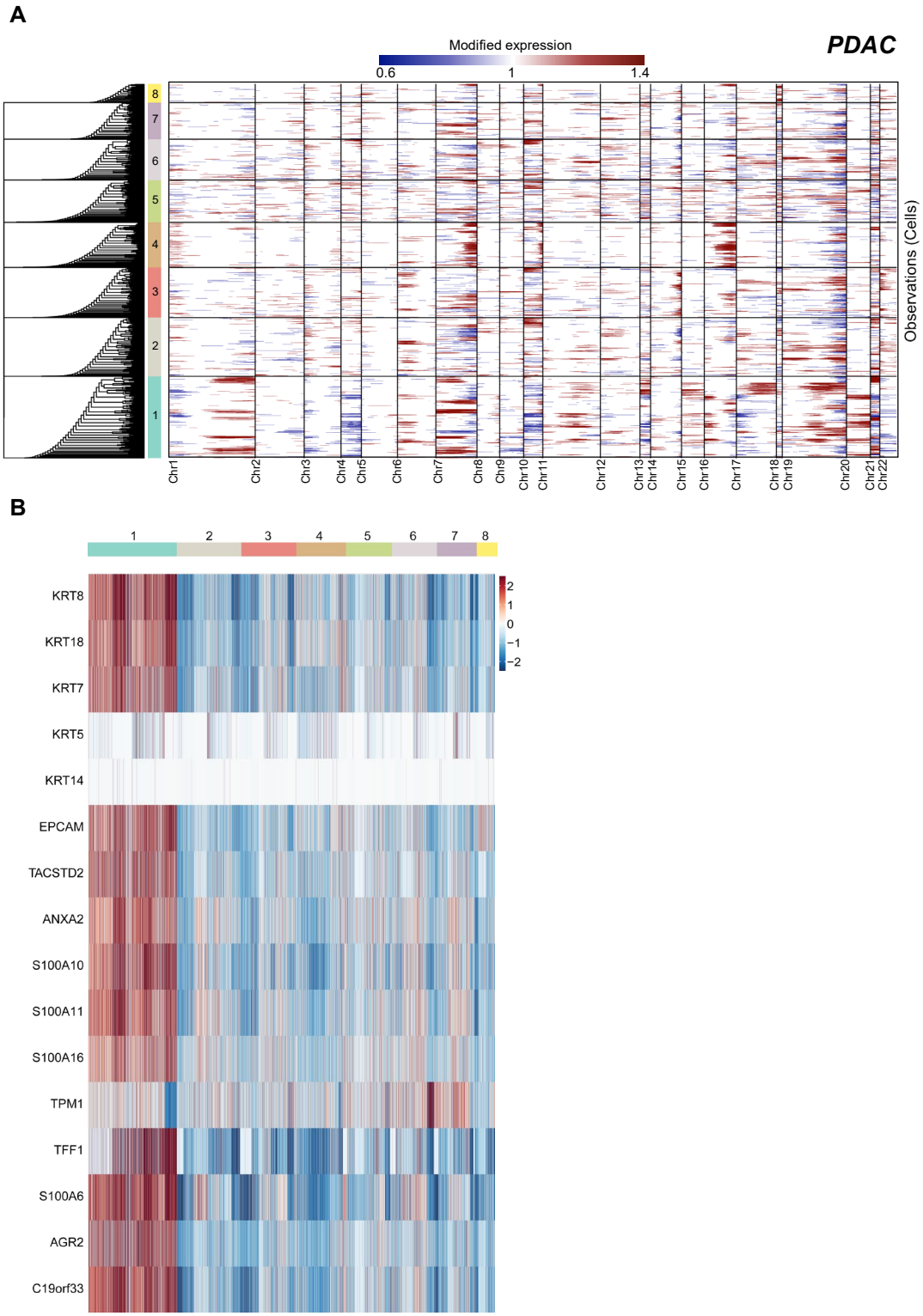
H&E: Tissues were fixed in 10% neutral buffered formalin at room temperature for 24 h then placed in 70% ethanol until processing, which was normally within 24 h. A Tissue-Tek VIP autoprocessor (Sakura, Torrance, CA) was used to process tissues that were then embedded in Paraplast (melting temperature 56–60°C), sectioned to 4 μm and mounted on glass slides. Sections were stained with hematoxylin and eosin (H&E) for pathologic analysis.

Network analysis: Network analysis was performed with the Ingenuity Pathway Analysis program (Qiagen, CA) and R programming. Differential expression was first performed with FindMarkers function in Seurat with R on comparison groups. The differential expression matrices were then imported into the Ingenuity Pathway Analysis program. Pathway construction began by adding genes of interest (S100P, STAT3, CLDN4) as initial nodes in a pathway. Using the grow function in the Ingenuity Pathway Analysis program, 10 direct and indirect upstream and downstream pathways based on differential expression data, human species, and cancer related databases were specified to autogenerate gene pathways. The levels of fold change were plotted with R using ggplot plotting language and compared with Tukey's multiple comparison t test.

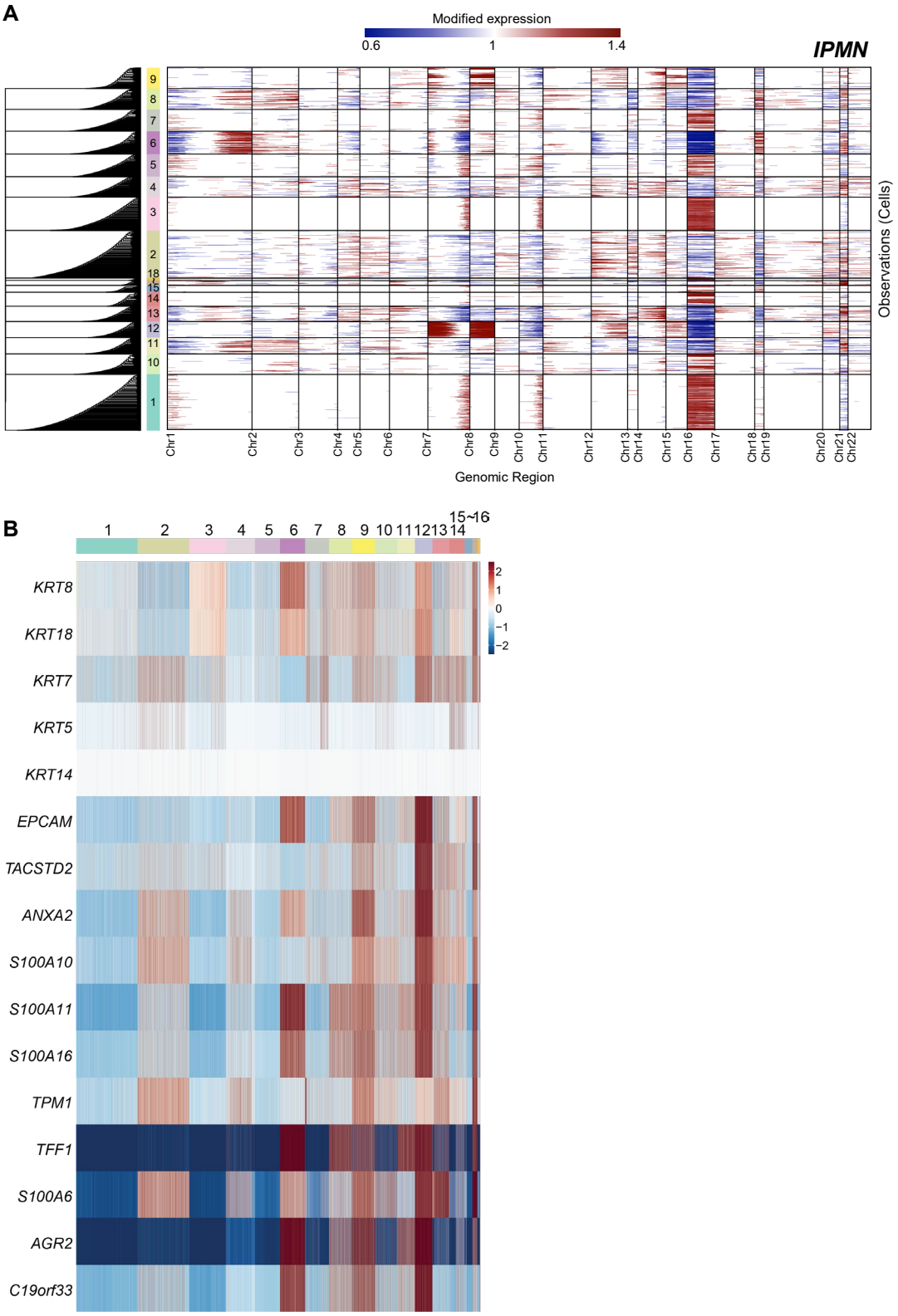
Supplementary Figures



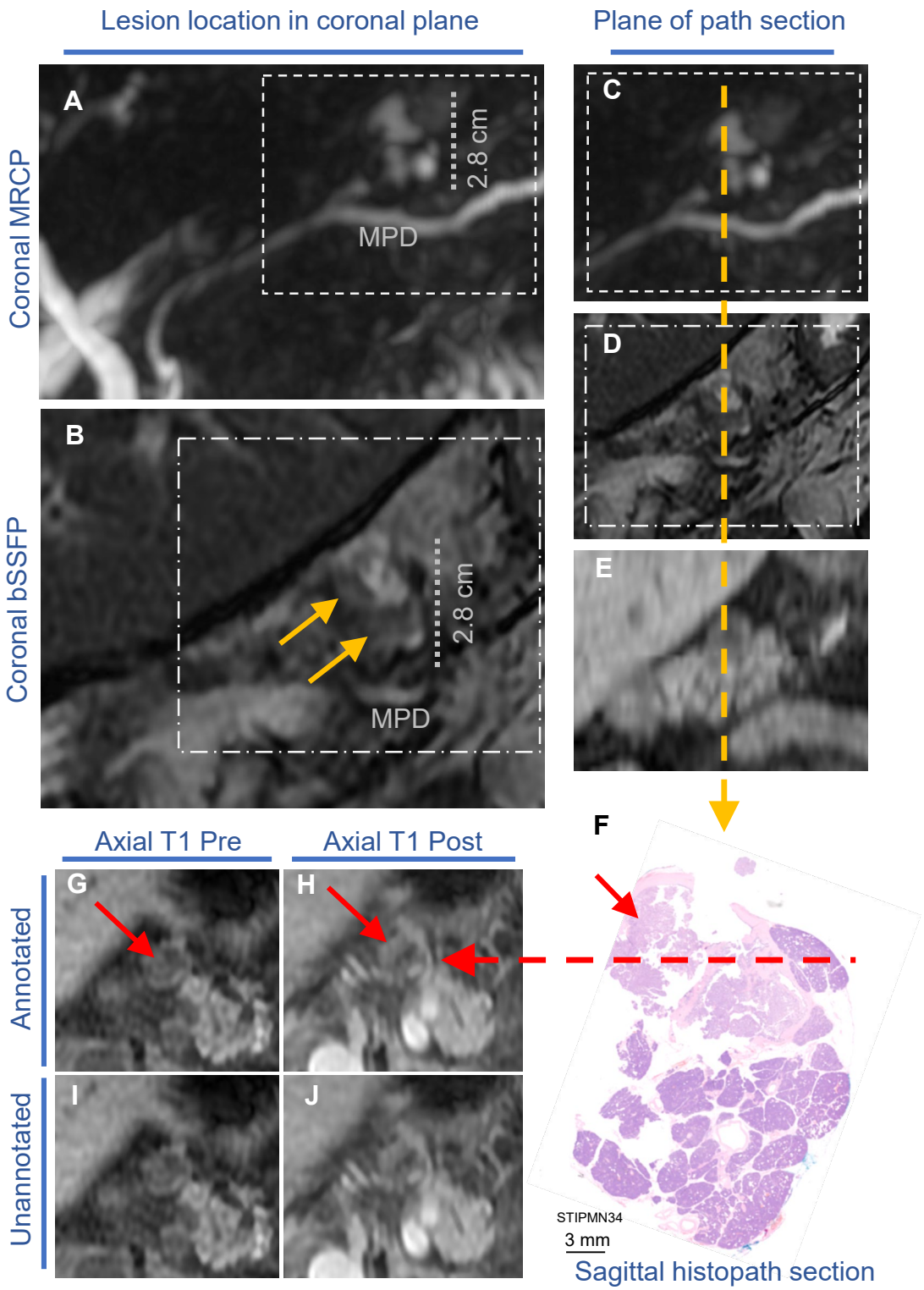
Supplementary Fig. 1. Heatmap for all pancreatic clusters in PDAC and the corresponding cell types. A) Top) Summary method schematic of the paper. Bottom) Summary of the PDAC samples and corresponding treatments. B) Heatmap of top cluster top differentially expressed genes and annotated based on scRNA sequencing. C) Clustering and overlap of clusters on histology sections. D) Differential expression between clusters were compared with scRNA cell type signatures using a one-sided hypergeometric t test.



Supplementary Fig. 2. Copy number variation (CNV) and tumor signature genes plotted against clusters in PDAC. A) Red to blue color bar represents the scale of the output of normalized and centered expression smoothed using a moving average filter with a width of 100 genes, which indicates copy number gains and losses. CNV was calculated by comparing each cluster to the average across clusters. B) Heatmap of PDAC clusters plotted using tumor signatures from scRNA confirms that cancer associated genes are enhanced in Cluster 1. Color bar indicates Z score.

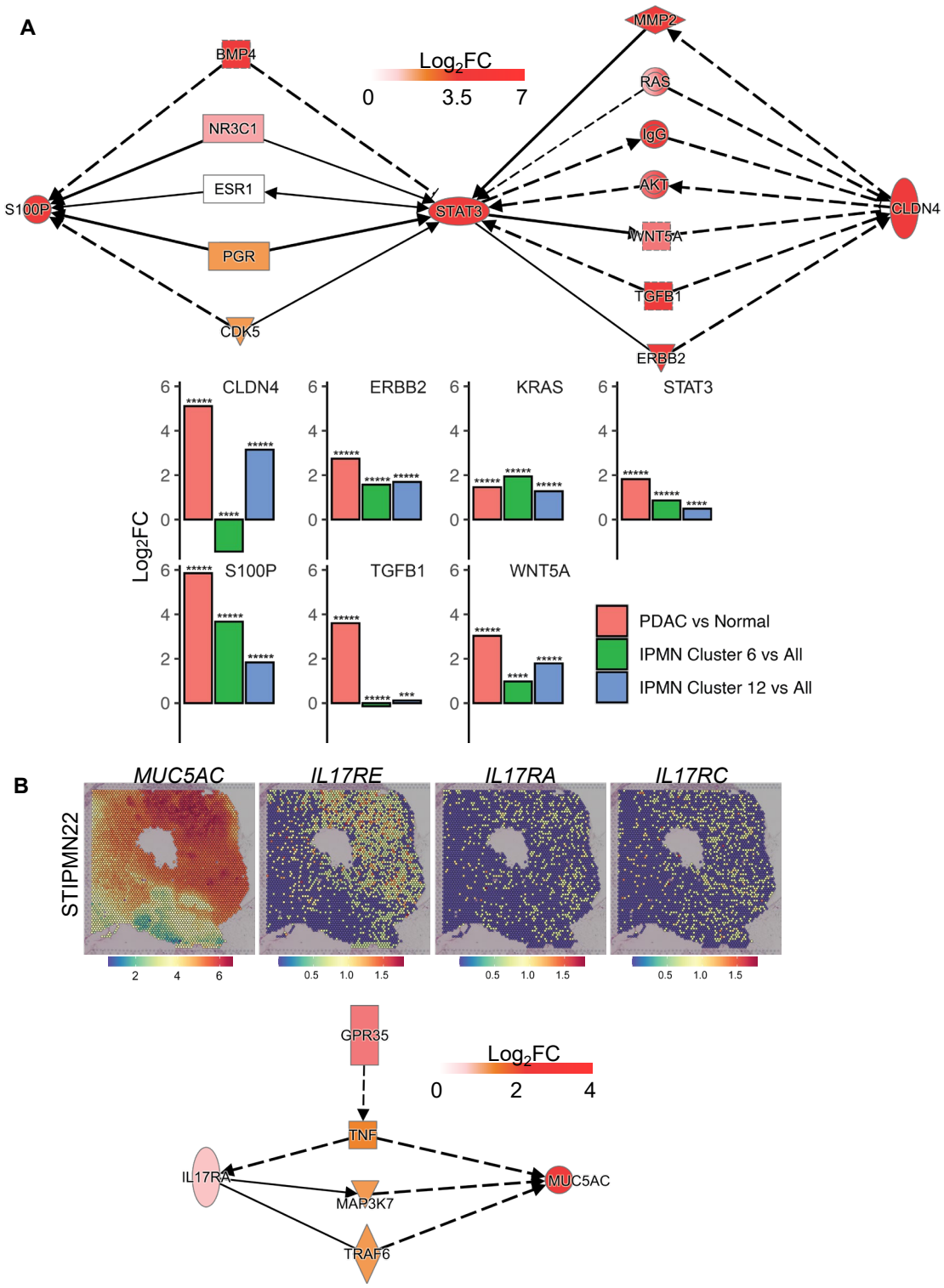


Supplementary Fig. 3. Copy number variation (CNV) tumor signature genes plotted against clusters in IPMN. A) Red to blue color bar represents the scale of the output of normalized and centered expression smoothed using a moving average filter with a width of 100 genes, which indicates copy number gains and losses. CNV was calculated by comparing each cluster to the average across clusters. B) Heatmap of IPMN clusters plotted using tumor signatures from scRNA. Color bar indicates Z score.

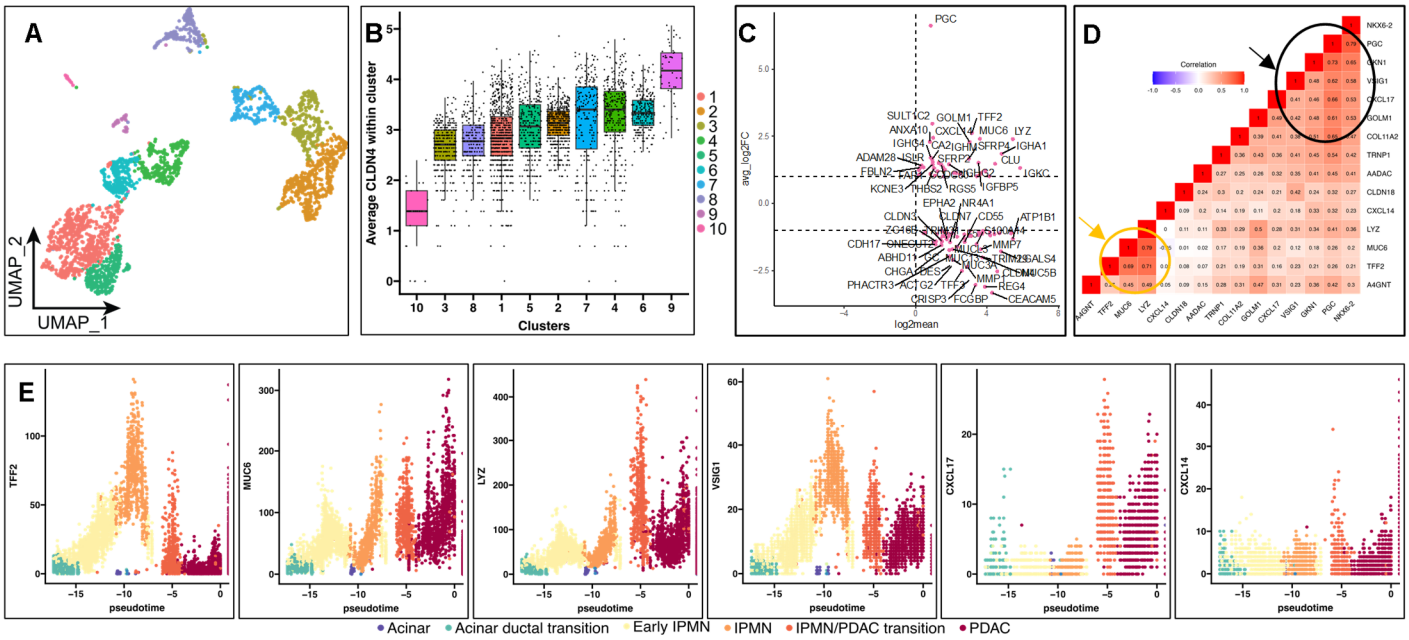


Supplementary Fig. 4. Corresponding magnetic resonance imaging (MRI) of IPMN sections near STIPMN34 tissue. Large (A) and small (C) field-of-view images from the coronal T2-weighted magnetic resonance cholangiopancreatography (MRCP). Large (B) and small (D) field-of-view images from the coronal balanced steady state free precession (bSSFP). The IPMN measures about 2.8cm in size and is characterized by high signal on the T2 weighted MRCP. The solid yellow arrows (B) point to tissue with intermediate signal along the superior margin of the IPMN, distinct from higher signal seen in the normal pancreatic tissue. (E) Coronal T1-weighted image during peak pancreatic enhancement (ppe) following injection of gadolinium-based contrast agent (GBCA). The dashed yellow arrow indicates the plane of histopathologic section (F) through

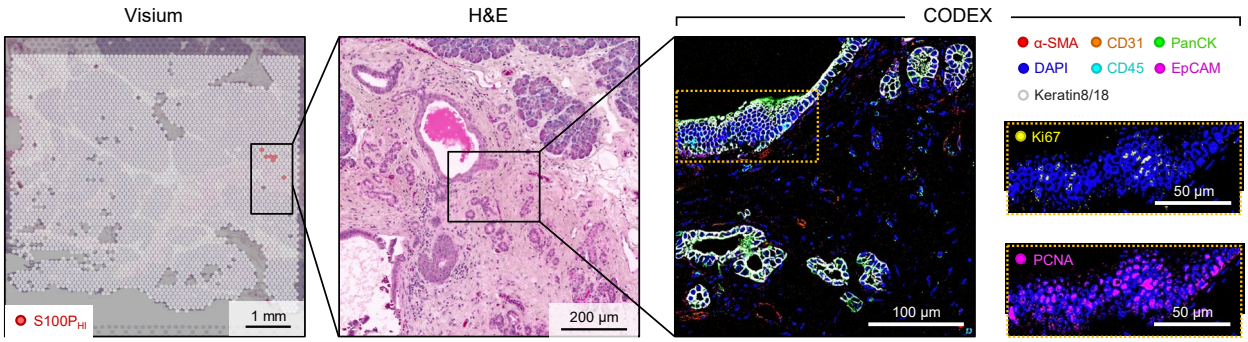
images C, D, and E, showing the region demonstrating an elevated cancer surfaceome score and elevated CLDN4 tissue is along the superior margin of the IPMN. Axial T1 weighted images pre-contrast (G, I) and post-GBCA during ppe (H, J) show a subtle area of low-grade enhancement (below that of normal pancreatic tissue) corresponds with this region of elevated cancer surfaceome score and elevated CLDN4 (solid red arrow). This enhancement pattern is typical of pancreatic adenocarcinoma. The dashed red arrow indicates the plane of images G and H through the histopathologic section (F). Both annotated (G,H) and unannotated (I,J) axial T1 weighted images are included for ease of review. MPD: Main Pancreatic Duct.



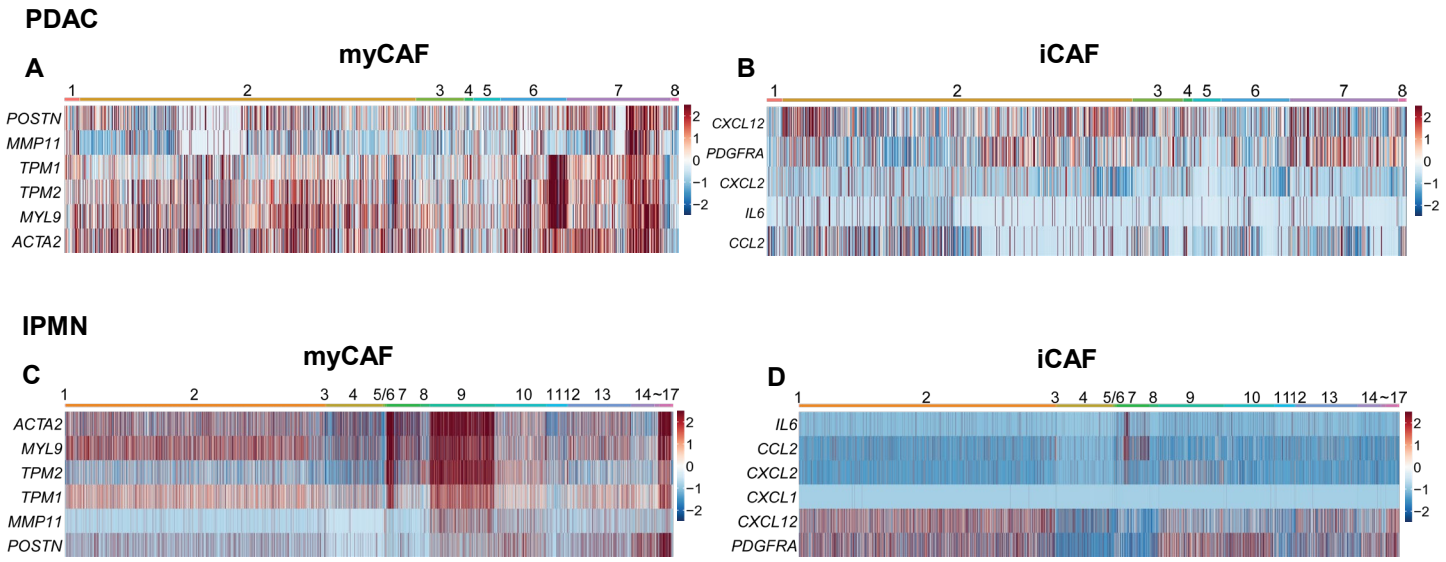
Supplementary Fig. 5. Gene network analysis. A) Gene network relating S100P and CLDN4 based on gene differential expression from PDAC vs Normal samples, IPMN cluster 6 vs remaining clusters, and IPMN cluster 12 vs remaining clusters. Log_2FC of genes within network were plotted and p values are: ***** $p < 10^{-100}$, **** $p<10^{-10}$, *** $p<0.005$. B) Given that MUC5AC is differentially expressed in the IPMN and PDAC lesions, we investigated the expression network and found IL17 to be a major component. IPMN spatial transcriptomic data for MUC5AC and IL17RA, IL17RC and IL17RE demonstrates the expression of the IL17 receptors. Below) IL-17RA and MUC5AC gene network. Arrows represent activation and flat end represent inhibition. Solid line is direct relationship, and dashed line is indirect relationship. Intensity scale bar represents Log_2FC. Differential expression was done with non-parametric ranked-sum Wilcoxon test with Bonferroni correction for p values.



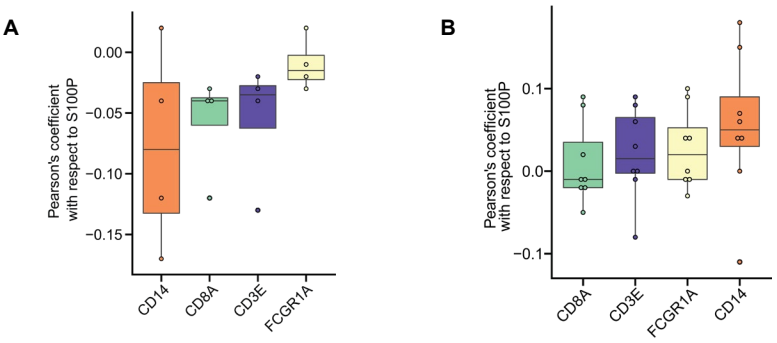
Supplementary Fig. 6. Analysis of cellular subsets within Cluster 1 (Fig. 1) with low CLDN4 expression. A) Uniform Manifold Approximation and Projection (UMAP) of subclusters. B) CLDN4 expression within subclusters. C) Differential gene expression for subcluster 10 as compared with the remainder of Cluster 1. D) Pearson's correlation of mRNA expression within genes enhanced in subcluster 10 (lower CLDN4 expression). Color bar represents Pearson's correlation value ranging from -1 to 1. E) Pseudotime analysis of genes with enhanced expression in subcluster 10 (Panels from left to right are labeled on the y axis and are *TFF2*, *MUC6*, *LYZ*, *VSIG1*, *CXCL17*, *CXCL14*, respectively). n = 7 samples were used in this analysis. Differential expression was done with non-parametric ranked-sum Wilcoxon test with Bonferroni corrected p values.



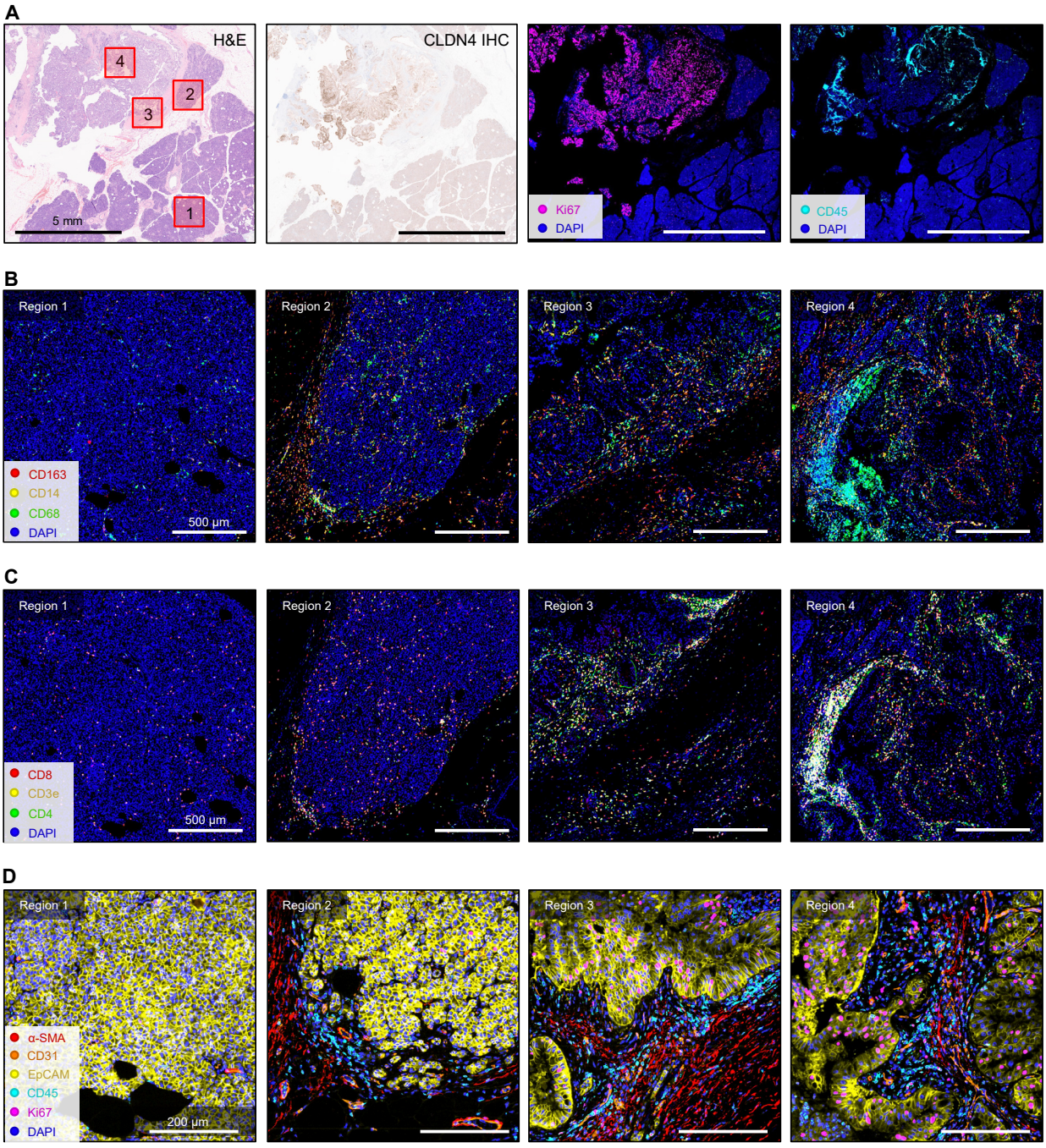
Supplementary Fig. 7. Spatial transcriptomics/CODEX imaging of small ductal lobules demonstrating sensitivity of each technique. Combining spatial proteomics and transcriptomics enhanced the detection of small ductal lobules that were located in the pancreas surrounding IPMN lesions. These small lesions were considered to be precancers based on nuclear morphology and H&E. In spatial transcriptomics, these lesions expressed *S100P* and *MUC5AC* but not *CLDN4*.



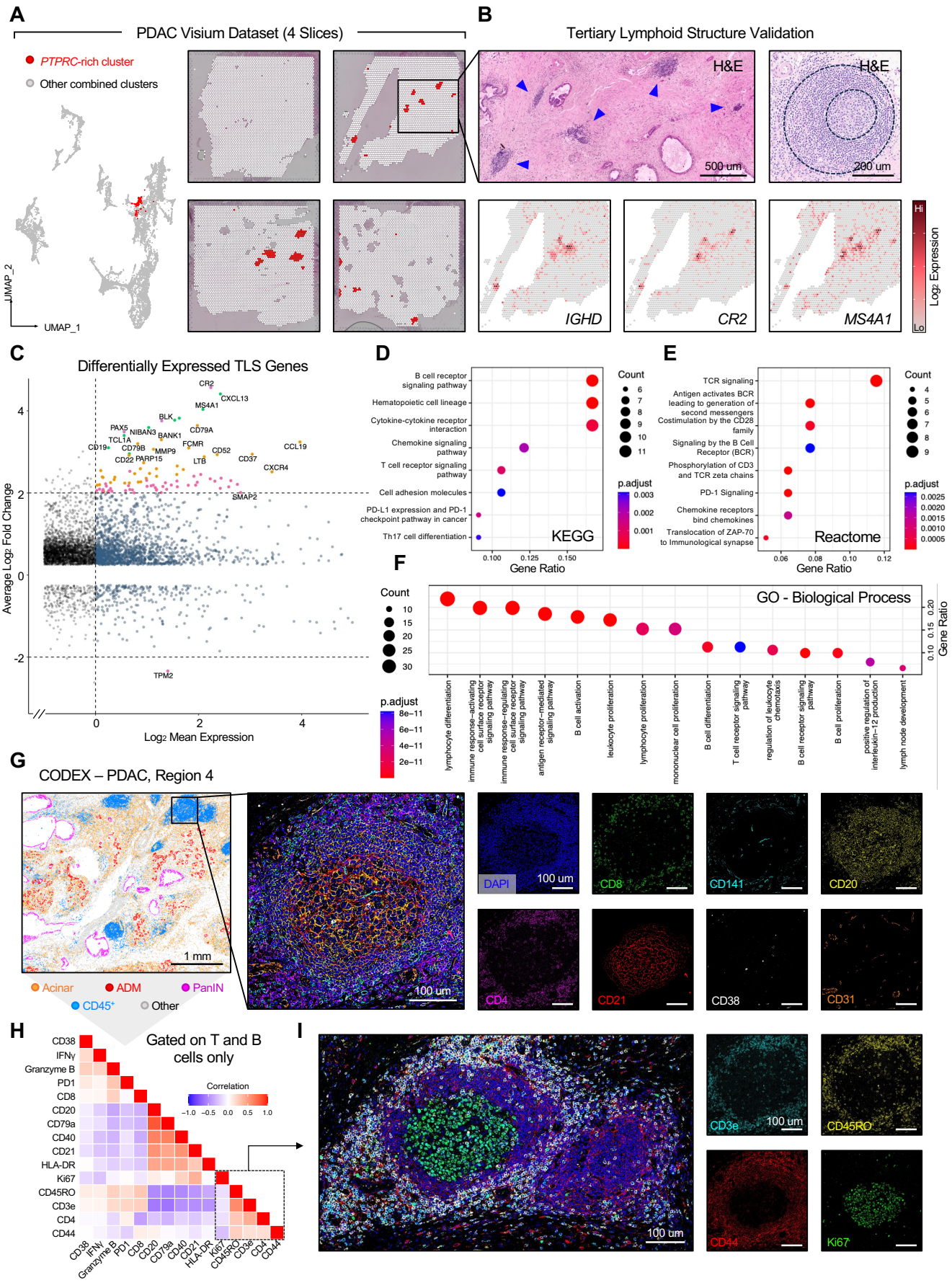
Supplementary Fig. 8. Cancer-associated fibroblast (CAF) heatmaps across Visium clusters based in PDAC and IPMN with CAF signature gene sets detailed in [1]. A-B) Heatmap of PDAC clusters plotted using (A) myCAF and (B) iCAF gene signatures from [1]. C-D) Heatmap of IPMN clusters plotted using (C) myCAF and (D) iCAF gene signatures from [1]. Color bar in heatmap indicates Z score.



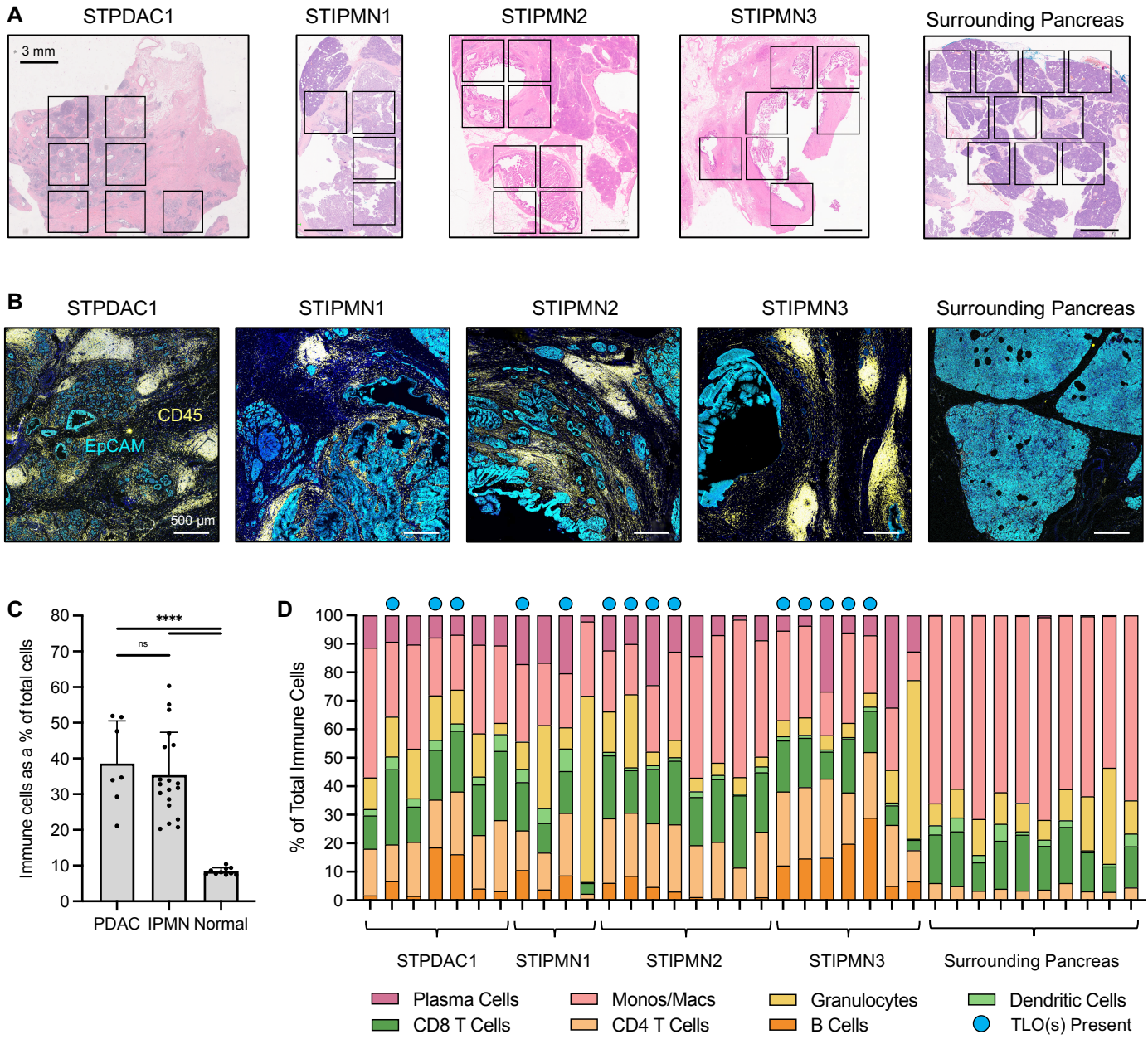
Supplementary Fig. 9. Correlation of immune cell markers with S100P. A-B) Pearson's coefficient for the spatial correlation of immune cell markers (*CD3, CD8, CD64 (FCGR1A), CD14*) and S100P. A) PDAC samples, B) IPMN samples.



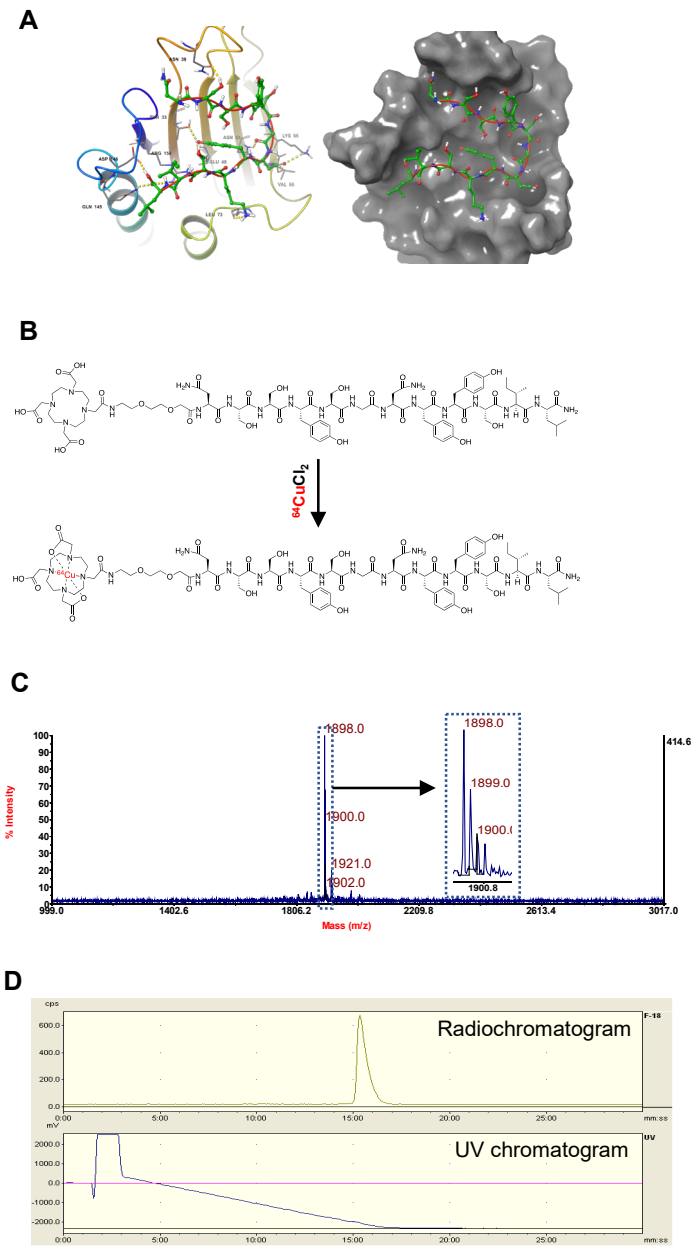
Supplementary Fig. 10. CODEX imaging of IPMN. A) Region layout of H&E and CLDN4 IHC, with Ki67 and CD45 CODEX expression maps. B-C) Regional mapping showing B) myeloid markers and C) T cell markers. D) Regional magnification showing epithelial, proliferation, and vessel marker expression, demonstrating regional variability throughout the IPMN.


A
PDAC Visium Dataset (4 Slices)
PTPRC-rich cluster
Other combined clusters
UMAP_2
UMAP_1
B
Tertiary Lymphoid Structure Validation
H&E
500 um
H&E
200 um
IGHD
CR2
MS4A1
Hi
Lo
Log2 Expression
C
Differentially Expressed TLS Genes
Average Log2 Fold Change
Log2 Mean Expression
CR2
CXCL13
MS4A1
BLK
CD79A
PAX5
NIBAN3
BANK1
TCL1A
CD19
CD79B
FCMR
MMP9
CD52
CCL19
CD22
PARP15
LTB
CD37
CXCR4
SMAP2
TPM2
D
B cell receptor signaling pathway
Hematopoietic cell lineage
Cytokine-cytokine receptor interaction
Chemokine signaling pathway
T cell receptor signaling pathway
Cell adhesion molecules
PD-L1 expression and PD-1 checkpoint pathway in cancer
Th17 cell differentiation
KEGG
Gene Ratio
Count
p.adjust
E
TCR signaling
Antigen activates BCR leading to generation of second messengers
Costimulation by the CD28 family
Signaling by the B Cell Receptor (BCR)
Phosphorylation of CD3 and TCR zeta chains
PD-1 Signaling
Chemokine receptors bind chemokines
Translocation of ZAP-70 to Immunological synapse
Reactome
Gene Ratio
Count
p.adjust
F
GO - Biological Process
Count
p.adjust
Gene Ratio
lymphocyte differentiation
immune response-activating cell surface receptor signaling pathway
immune response-regulating cell surface receptor signaling pathway
antigen receptor-mediated signaling pathway
B cell activation
leukocyte proliferation
lymphocyte proliferation
mononuclear cell proliferation
B cell differentiation
T cell receptor signaling pathway
regulation of leukocyte chemotaxis
B cell receptor signaling pathway
B cell proliferation
positive regulation of interleukin-12 production
lymph node development
G
CODEX – PDAC, Region 4
1 mm
100 um
Acinar
ADM
PanIN
CD45+
Other
DAPI
100 um
CD8
CD141
CD20
CD4
CD21
CD38
CD31
H
Gated on T and B cells only
Correlation
CD38
IFNγ
Granzyme B
PD1
CD8
CD20
CD79a
CD40
CD21
HLA-DR
Ki67
CD45RO
CD3e
CD4
CD44
I
100 um
CD3e
100 um
CD45RO
CD44
Ki67

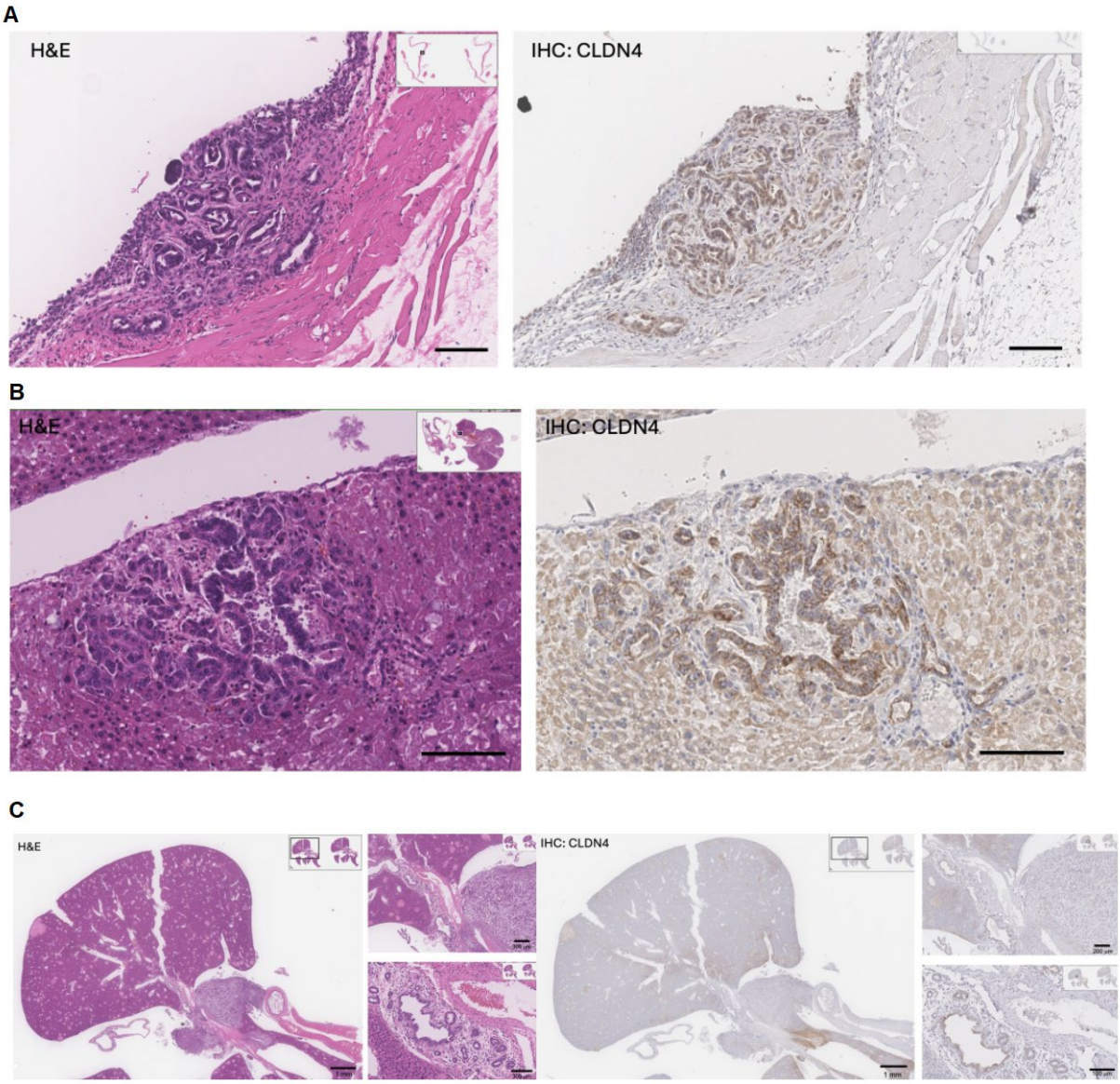
Supplementary Fig. 11. CODEX imaging of tertiary lymphoid organs (TLOs). A) Four spatial transcriptomic PDAC regions were merged, normalized with the SCTransform function, and clustered with Seurat. The *protein tyrosine phosphatase receptor type C* (*PTPRC, CD45*)-rich cluster in the dataset was highlighted in red both on Uniform Manifold Approximation and Projection (UMAP) and in spatial transcriptomic coordinates, corresponding to TLOs. B) Overlapping H&E and B-cell gene signatures confirm the presence of TLOs (blue arrowheads). C) Magnitude and average (MA) plot of differentially-expressed genes (DEGs) in the *PTPRC*-rich/TLO cluster in comparison to the rest of the PDAC spatial transcriptomic dataset. D) KEGG, E) REACTOME, and F) GO – Biological Process Pathway analysis of DEGs > average $\log_2$ fold change of 2 from (C). G) CODEX imaging of TLO and several immune surface receptors from a representative PDAC region. H) Pearson's correlation of several surface markers expressed on T and B cells from the PDAC region in (G). I) CODEX imaging of the memory T-cell shell and proliferating B-cell core of a TLO, validating the Pearson's correlation from (H).



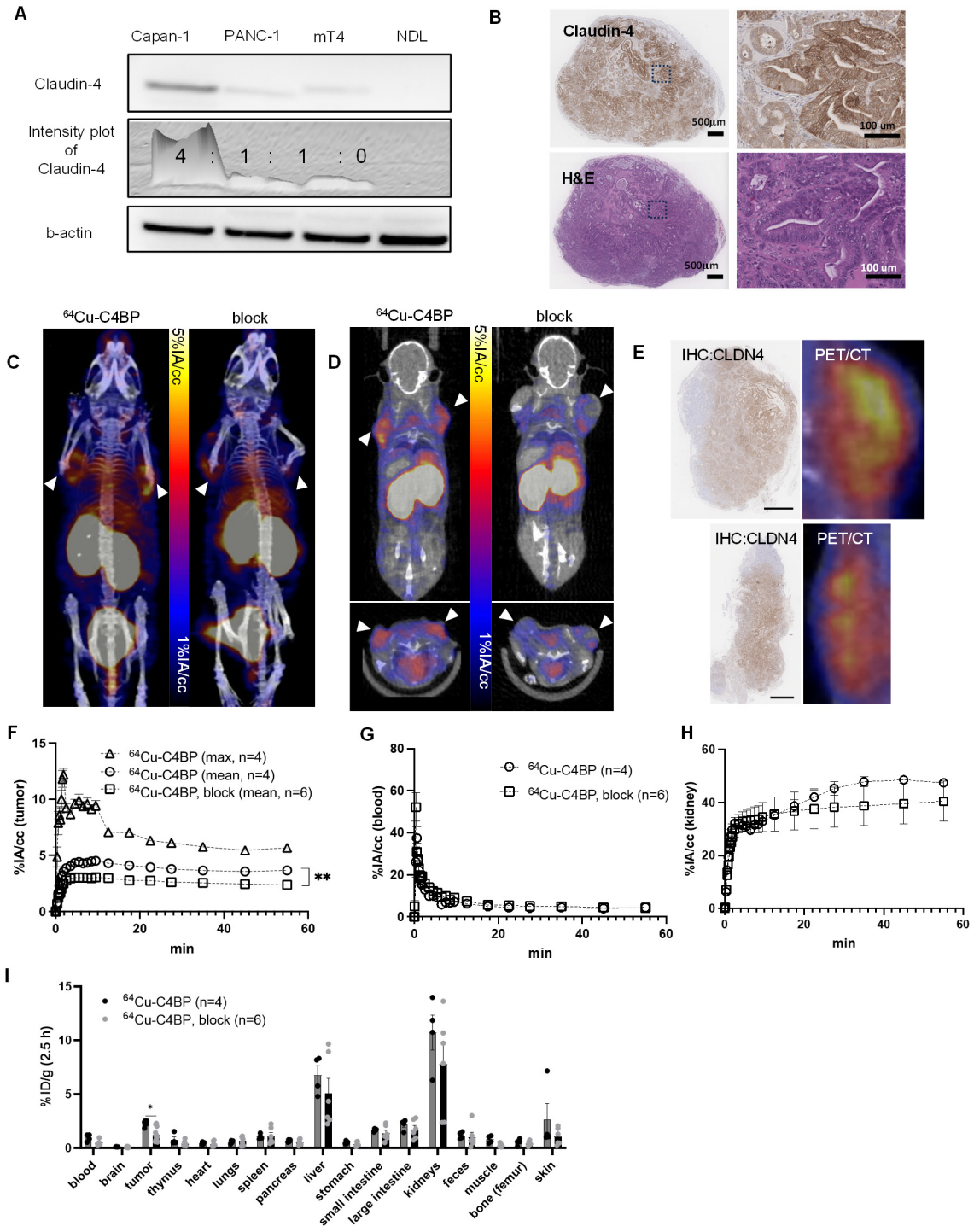
Supplementary Fig. S12. CODEX imaging and analysis ofmmune cells across PDAC and IPMN. A) IHC of target regions. B) CODEX imaging of DAPI (dark blue), EpCAM (light blue) and CD45 (yellow) for regions of PDAC, IPMN and surrounding pancreas. C) Overall fraction of immune cells across all fields. D) Quantification of immune cell phenotype for varied fields and identification of regions containing at least 1 TLO. One-way ANOVA results are as follows for C): **** = p<0.0001, ns = not significant.



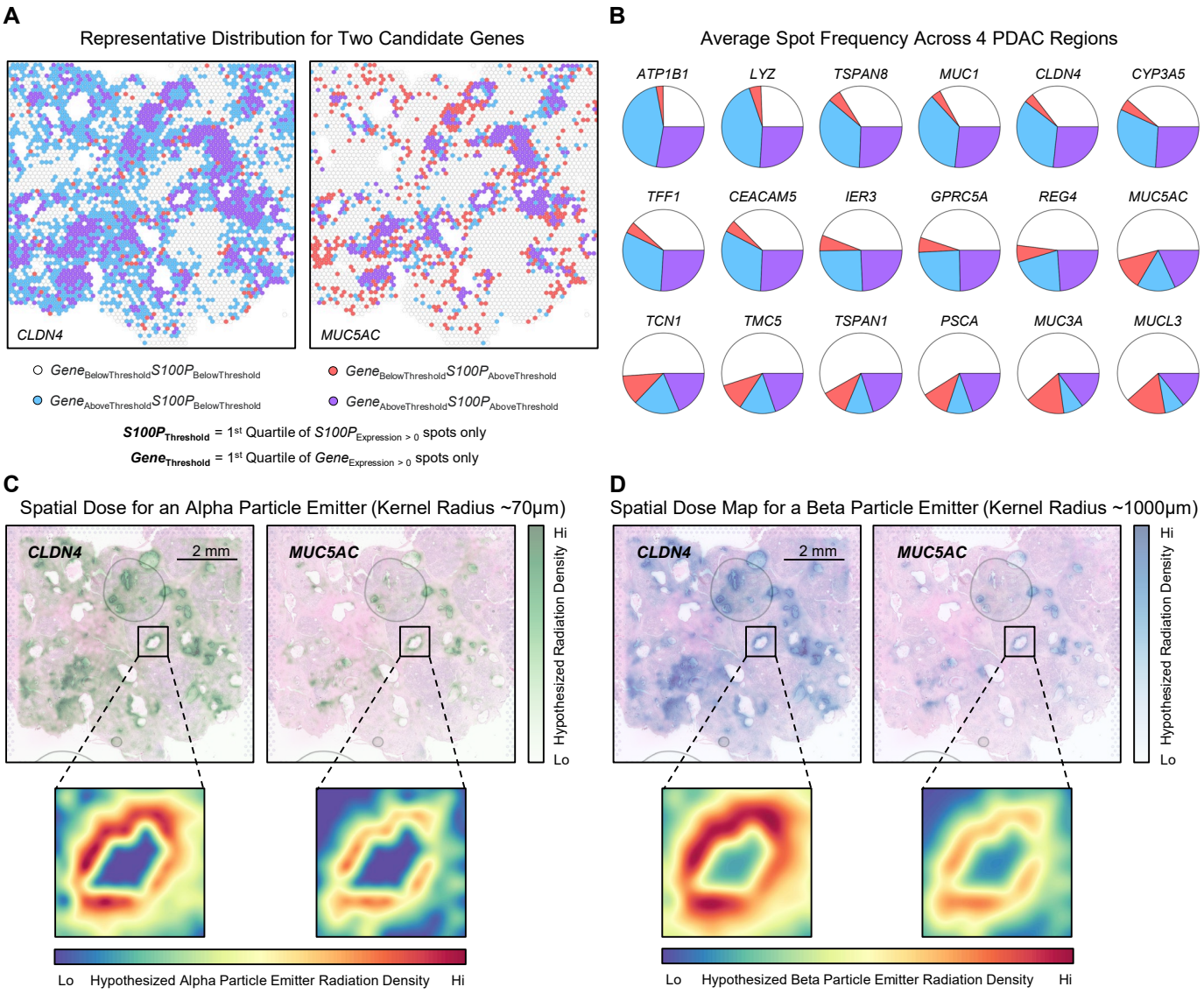
Supplementary Fig. 13. Peptide targeting of claudin-4. A) Modeling demonstrates the NSSYSGNYYSIL peptide in binding pocket. B) ^{64}Cu-labeling scheme. C) MALDI mass spectrum of DOTA-PEG$_2$-C4BP. D) Radio- and UV-chromatogram of ^{64}Cu-C4BP.



Supplementary Fig. 14. H&E and CLDN4 immunohistochemistry staining of mouse intestines, pancreas, and liver. H&E and CLDN4 staining of A) small intestines and B) liver presenting a metastasized tumor (Scale bar, 0.1 mm). C) H&E and CLDN4 staining of liver and adjacent tissues displaying high CLDN4 expression.



Supplementary Fig. 15. Molecular imaging of claudin-4 in a human xenograft mouse model. A) Expression of claudin-4 in various cell lines (Capan-1: human pancreatic adenocarcinoma cell line, PANC-1: human pancreatic cancer cell line, mT4: murine pancreatic cancer cell line, NDL: mouse mammary carcinoma cell line). B) CLDN4 IHC and H&E in Capan-1 tumors. C) Representative MIP PET/CT image of xenograft mouse bearing Capan-1 tumors. Image represents ^{64}Cu-C4BP retention in tumors at 30-60 min post injection. D) PET/CT slice images with and without co-injection of 500-fold excess of cold peptide for blocking. White arrowheads in C) and D) indicate tumors. E) Comparison of IHC and PET/CT images. Spatial intensity map of CLDN4-antibody and ^{64}Cu-C4BP within tumor (Scale bar: 1 mm). F-H) Time activity curves (TACs) for ^{64}Cu-C4BP concentration in F) tumor, G) blood and H) kidney from the PET image of dynamic scan for 1 hour post injection. I) Biodistribution of ^{64}Cu-C4BP on organs obtained at 2.5 hours post injection. Graphs are presented as mean±s.e.m. Unpaired two-tailed was performed in (F, multiple t-test with multiple comparison correction) and (I) (* = $p<0.05$, ** = $p<0.01$).



Supplementary Fig. 16. Modeling of claudin-4 radiopharmaceutical distribution for future therapeutic applications. A) Visium spots for a representative PDAC region were colored using the 1st quartile of gene/*S100P* expression as a threshold, demonstrating that a claudin-4/mucin-5ac specific theragnostic agent would detect all S100P expressing cells (purple) and additional cells (blue). The spots in red contain *S100P* but not *CLDN4* or *MUC5AC*, representing areas that would be missed after administering a theragnostic. B) Similar analysis to (A) for select cancer-upregulated genes averaged across four PDAC regions. C-D) Representative 2D microdosimetry maps for C) alpha (211At) and D) beta (177Lu) emitters targeted to either CLDN4 or MUC5AC. The relative dose distribution was estimated in 2D by convolution of the gene expression map with isotope-specific dose point kernels. Color bars represent radiation intensity with arbitrary units.

Supplementary Tables

Supplementary Table 1. Clinical data regarding patient samples acquired at Stanford University and from Ref. 23 and 24. Fifteen female and thirteen male patients were included in the analysis, with an overall median age of 72 and an age range from 51 to 89 years-old.

Sample	Grade	Location	Diabetes
LG_1	LG IPMN	head	No
LG_2	LG IPMN	head	Yes
LG_3	LG IPMN	head, body	Yes
LG_4	LG IPMN	head	Yes
LG_5	LG IPMN	body/tail	Yes
LG_6	LG IPMN	body/tail	No
LG_7	LG IPMN	body/tail	No
HG_1	HG IPMN	head	No
HG_2	HG IPMN	head	No
HG_3	HG IPMN	head	No
PDAC_1	PDAC	Head	No
PDAC_2	PDAC	Head, Uncinate	Yes
PDAC_3	PDAC	head	Ues
HT264P1	PDAC	body	No
HT270P1	PDAC	Head	Type II
HT284P1	PDAC	neck/body margin	Type II
HT288P1	PDAC	Head	Type II
HT224P1	PDAC	Head	Type II
HT231P1	PDAC	Tail	No
HT231P1-2	PDAC	Tail	No
HT232P1	PDAC	body/tail	No
HT232P1-2	PDAC	body/tail	No
HT259P1	PDAC	Head	No
HT306P1	PDAC	Head	No
HT306P1-2	PDAC	Head	No
HT306P1-3	PDAC	Head	No
HT306P1-4	PDAC	Head	No
HT242P1	PDAC	Tail (proximal remnant)	Yes
STPDAC11	PDAC	Head	Type II (2 mos)
STPDAC12	PDAC	Head	Type II (2 mos)
STPDAC13	PDAC	Head	Type II (2 mos)
STPDAC14	PDAC	Head	Type II (2 mos)
STIPMN11	HG IPMN	Head	Prediabetes
STIPMN12	HG IPMN	Head	Prediabetes
STIPMN21	HG IPMN	Body/tail	Type II (2 mos)
STIPMN22	HG IPMN	Body/tail	Type II (2 mos)
STIPMN31	HG IPMN	Tail	No
STIPMN32	HG IPMN	Tail	No
STIPMN33	HG IPMN	Tail	Prediabetes
STIPMN34	HG IPMN	Tail	Prediabetes

Supplementary Table 2. Genes from cancer surfaceome with greater than 80% frequency of expression in pancreatic cancer.

B2M	100.00
EEF1A1	99.99
S100A6	99.94
HLA-A	99.35
CD63	98.65
ITM2B	98.63
HLA-C	98.41
IFITM3	98.34
SPINT2	97.90
RAC1	97.73
HSP90AA1	97.55
CD74	97.29
EPCAM	96.18
TM4SF1	96.16
CYBA	96.10
CD59	95.89
RPSA	95.73
HSP90AB1	94.15
ATP1A1	93.57
ATP1B1	93.26
VAMP8	92.40
LY6E	92.10
TSPAN8	90.40
ARF1	89.77
HLA-E	89.27
RHOA	89.18
CDC42	89.04
CLDN4	88.83
CD151	88.61
TACSTD2	88.23
CIB1	87.51
IFITM2	87.32
CD164	86.53
ITGB1	86.47
APLP2	86.33
CD9	86.33
RTN4	86.27
ENO1	86.15
UBE2D3	86.12
CALR	85.88
RAB11A	85.57
APP	85.51
MUC1	85.32
TSPAN3	85.24
EZR	85.06
BSG	85.03
VDAC1	84.98
P4HB	84.87
HLA-DRA	84.85
TMEM123	84.52
TMED10	83.19
VAPA	81.93
VPS28	81.55
TMEM219	81.32
MAL2	81.02
CLDN7	80.28
HLA-B	80.05

Supplementary Table 3. Top fold change genes that were also cancer surfacesome genes from cluster 1 in PDAC. Differentially expressed genes were filtered to have a p adjusted value of less than 0.005, $\log_2$ fold change of greater than 2, and only cancer surfacesome genes. p adjusted values were based on a non-parametric ranked-sum Wilcoxon test with Bonferroni correction.

Gene	avg_log2FC	p_val_adj
CLDN4	13.9490565	<7.6E-300
MUC1	12.9688808	<7.6E-300
S100A6	12.0459834	<7.6E-300
ATP1B1	11.9892492	<7.6E-300
EPCAM	8.16324381	<7.6E-300
TSPAN3	7.09969735	<7.6E-300
TACSTD2	6.64513503	<7.6E-300
MAL2	6.62702882	<7.6E-300
SPINT2	5.69193482	<7.6E-300
TM4SF1	5.61342856	<7.6E-300
TSPAN8	5.47374558	<7.6E-300
CD151	5.10789781	<7.6E-300
CD164	3.66450756	<7.6E-300
ATP1A1	3.44909867	<7.6E-300
HSP90AA1	2.99706639	<7.6E-300
BSG	2.77598458	<7.6E-300
CLDN7	2.60022171	<7.6E-300
APLP2	2.5657688	<7.6E-300
CD9	2.41776531	<7.6E-300
VDAC1	2.16868499	<7.6E-300
TMEM123	2.08693183	<7.6E-300

Supplementary Table 4. Biodistribution of ^{64}Cu-C4BP (given as %IA/g) in organs of interest at 22h.

	KT;Ptf1a^{CreER};Trp53$^{fl/fl}$ (n=3)		Wild type (n=3)		
	Mean	Stdev	Mean	Stdev	P value
blood	1.60	1.84	0.20	0.01	0.256
heart	1.23	0.59	0.29	0.05	0.051
lungs	0.89	0.09	0.50	0.20	0.036
liver	7.73	5.35	1.80	0.56	0.129
pancreas	1.46	0.86	0.16	0.02	0.058
spleen	1.27	0.63	0.24	0.03	0.045
stomach	0.54	0.24	0.60	0.16	0.778
small intestine	2.45	1.31	0.80	0.15	0.095
large intestine	4.08	2.64	0.90	0.17	0.106
feces	1.92	1.12	1.13	0.49	0.324
kidneys	6.57	3.85	1.14	0.13	0.071
muscle	0.38	0.16	0.10	0.01	0.041
bone (femur)	0.55	0.25	0.13	0.08	0.051
skin	0.78	0.43	0.20	0.04	0.080
brain	0.16	0.08	0.06	0.00	0.088
pancreas/muscle	3.71	0.56	1.53	0.10	0.003

Supplementary Table 5. Genes with enhanced expression in subcluster 10 compared with the remainder of cluster 1 from Figure 1 (restricted to genes with average log_2 fold change greater than 1.5 and adjusted p value below 0.05).

Gene	Average log_2 fold change	Adjusted p value
PGC	6.61080985	6.57E-34
SULT1C2	2.9686981	1.30E-16
TFF2	2.62198568	3.28E-14
VSIG1	2.55354617	8.11E-23
CXCL14	2.44793598	2.43E-13
MUC6	2.40624072	1.85E-13
LYZ	2.3957633	1.11E-14
ANXA10	2.29393608	5.76E-16
GOLM1	2.28199427	1.29E-15
CXCL17	2.13658978	9.47E-36
TRNP1	2.08757002	1.26E-19
ADH1C	2.02782329	4.67E-18
NKX6-2	2.010595	2.25E-226
A4GNT	1.8987742	3.17E-29
IGHA1	1.84919811	2.05E-10
GKN1	1.71511309	0
MFAP5	1.71138147	1.21E-22
ALDH3A1	1.7084192	3.05E-27
IGHG4	1.70636113	9.34E-11
SFRP4	1.65802546	3.89E-10
PIK3C2G	1.64872981	2.08E-14
CA2	1.6393763	1.80E-13
CLDN18	1.56122327	2.60E-15
ISLR	1.54309321	4.99E-08
AADAC	1.51937112	1.57E-41
IGFBP5	1.5173545	1.66E-06
SFRP2	1.51135135	1.01E-07

References

1 Han, C., Liu, T. & Yin, R. Biomarkers for cancer-associated fibroblasts. *Biomarker Research* **8**, 64, doi:10.1186/s40364-020-00245-w (2020).